

SUPERNOVA LIGHT CURVES POWERED BY YOUNG MAGNETARS

DANIEL KASEN^{1,3} AND LARS BILDSTEN²

¹ Department of Astronomy and Astrophysics, University of California, Santa Cruz, CA 95064, USA

² Kavli Institute for Theoretical Physics and Department of Physics, Kohn Hall, University of California, Santa Barbara, CA 93110, USA

Received 2009 October 30; accepted 2010 April 13; published 2010 June 10

ABSTRACT

We show that energy deposited into an expanding supernova remnant by a highly magnetic ($B \sim 5 \times 10^{14}$ G) neutron star spinning at an initial period of $P_i \approx 2\text{--}20$ ms can substantially brighten the light curve. For magnetars with parameters in this range, the rotational energy is released on a timescale of days to weeks, which is comparable to the effective diffusion time through the supernova remnant. The late time energy injection can then be radiated without suffering overwhelming adiabatic expansion losses. The magnetar input also produces a central bubble that sweeps ejecta into an internal dense shell, resulting in a prolonged period of nearly constant photospheric velocity in the observed spectra. We derive analytic expressions for the light curve rise time and peak luminosity as a function of B and P_i , and the properties of the supernova ejecta that allow for direct inferences about the underlying magnetar in bright supernovae. We perform numerical radiation hydrodynamic calculations of a few specific instances and compare the resulting light curves to observed events. Magnetar birth is likely to impact more than a few percent of all core-collapse supernovae, and may naturally explain some of the brightest events ever seen (e.g., SN 2005ap and SN 2008es) at $L \gtrsim 10^{44}$ ergs s^{-1} .

Key words: radiative transfer – stars: neutron – supernovae: general – supernovae: individual (SN 2005ap, SN 2008es, SN 2007bi)

Online-only material: color figures

1. INTRODUCTION

Studies of soft gamma-ray repeaters and anomalous X-ray pulsars reveal that $\sim 10\%$ of newly born neutron stars (Kouveliotou et al. 1998) have dipole magnetic fields as high as $B \sim 10^{14}\text{--}10^{15}$ G for more than 1000 years after their birth (see Woods & Thompson 2006). These “magnetars” rotate at periods of $P = 5\text{--}12$ s at an age of 1000–10,000 years. Such highly magnetized neutron stars (NSs) were theoretically predicted (Duncan & Thompson 1992; Thompson & Duncan 1993), and most of their activity (both sporadic and persistent) must be powered by the decay of these large magnetic fields.

What remains unknown is just how highly magnetized and rapidly rotating these magnetars may be at “birth”. Many (see Bodenheimer & Ostriker 1974; Wheeler et al. 2000; Thompson et al. 2004) have investigated the possible impact on the central engine when the magnetar is so rapidly rotating (1–3 ms) and magnetized that its subsequent spin-down can power the explosion. Cases this extreme may also be sources for ultra-high energy cosmic rays (Arons 2003) or deposit enough energy in the collapsing stellar envelope to favorably shape the deep interior (Uzdensky & MacFadyen 2007; Bucciantini et al. 2009) for the production of a collimated relativistic flow needed for gamma-ray bursts. Such events depend on the combination of rapid rotation and high B to achieve a measurable effect during the few seconds critical to the core-collapse mechanism.

Building on the work of Gaffet (1977a, 1977b), we have found that weaker magnetic fields and less extreme spins (that do not alter the explosion mechanism) can dramatically impact supernova light curves, competing with the decay of radioactive ^{56}Ni and thermal energy in the expanding envelope. Maeda et al. (2007) previously raised this possibility for the Type Ib SN 2005bf, and Woosley (2009) has independently shown their relevance as well.

We show in Section 2 that when the timescale of the magnetar spin-down, t_p , is comparable to the effective radiative diffusion time, t_d , the resulting peak luminosity is $L_{\text{peak}} \sim E_p t_p / t_d^2$, where E_p is the magnetar rotational energy. Magnetars with 10^{13} G $< B < 10^{16}$ G and $P_i = 1\text{--}30$ ms can produce $L_{\text{peak}} > 10^{42}$ erg s^{-1} . We discuss the dynamics of the energy injection in Section 3 and show that the magnetar blows a central bubble in the SN ejecta, forming a dense inner shell of swept-up material which affects the spectroscopic evolution. In Section 4, we derive analytic expressions for the luminosity, L_{peak} , and duration, t_{peak} , of magnetar powered supernovae. We confirm these formulae with numerical radiation hydrodynamic calculations and show how they can be inverted to infer B and P_i from a given light curve. We close in Section 5 by discussing observed core-collapse SNe that may be powered this way, especially the ultra-bright SN 2005ap (Quimby et al. 2007) and SN 2008es (Gezari et al. 2009; Miller et al. 2009).

2. ENERGY DEPOSITION FROM A MAGNETAR: SIMPLE ESTIMATE

We first estimate the parameter space in which a magnetized NS is expected to influence the supernova light curve. This motivates the more detailed calculations given in the sections that follow. In the simplest model, the core-collapse mechanism has ejected an envelope of mass M_{ej} at a velocity v_t from a star of initial radius R_0 . Within a few expansion times, $t_e \sim R_0/v_t$, this ejecta will be undergoing self-similar adiabatic expansion, with an internal energy $E_{\text{int}} \sim E_{\text{sn}}(R_0/R)$, where $E_{\text{sn}} \sim M_{\text{ej}}v_t^2/2$ and $R \sim v_t t$ is the remnant size. In the absence of magnetar (or ^{56}Ni) heating, adiabatic expansion continues until the remnant is as old as the effective diffusion time $t_d \sim (\kappa M_{\text{ej}}/v_t c)^{1/2}$, where κ is the opacity, after which the entropy is lost. Such thermally powered light curves (e.g., Type IIp’s) have a luminosity $L_{\text{th}} \sim E_{\text{sn}} t_e / t_d^2$. The large amount

³ Hubble Fellow.

of adiabatic expansion that has occurred by the time $t \sim t_d$ leads to relatively low luminosities $L < 10^{43}$ ergs s^{-1} .

Now consider the impact of late time ($t \gg t_e$) energy injection from a young NS with radius $R_{\text{ns}} = 10$ km and initial spin $\Omega_i = 2\pi/P_i$. The rotational energy is

$$E_p = \frac{I_{\text{ns}}\Omega_i^2}{2} = 2 \times 10^{50} P_{10}^{-2} \text{ ergs}, \quad (1)$$

where $P_{10} = P_i/10$ ms; and we set the NS moment of inertia to be $I_{\text{ns}} = 10^{45}$ g cm^2 . This magnetar loses rotational energy at the rate set by magnetic dipole radiation (with the angle, α , between rotation and magnetic dipole given a fiducial value $\sin^2 \alpha = 1/2$), injecting most of the energy into the expanding remnant on the spin-down timescale

$$t_p = \frac{6I_{\text{ns}}c^3}{B^2 R_{\text{ns}}^6 \Omega_i^2} = 1.3 B_{14}^{-2} P_{10}^2 \text{ yr}, \quad (2)$$

where $B_{14} = B/10^{14}$ G. To input this energy at a time $t_p \lesssim t_d$ requires a minimum B field of

$$B > 1.8 \times 10^{14} P_{10} \kappa_{\text{es}}^{-1/4} M_5^{-3/8} E_{51}^{1/8} \text{ G}, \quad (3)$$

where we have scaled the parameters to typical supernova values $M_5 = M_{\text{ej}}/5 M_{\odot}$ and $E_{51} = E_{\text{sn}}/10^{51}$ ergs and assumed an opacity $\kappa_{\text{es}} = \kappa/0.2 \text{ cm}^2 \text{ g}^{-1}$ appropriate for electron scattering in an ionized plasma of electron fraction 1/2. The required fields are in the magnetar range. This late time entropy injection resets the interior energy scale to $E_{\text{int}} \sim E_p$ and overwhelms the initial thermal energy when $E_p > E_{\text{sn}}(t_e/t_p)$. Thus, even low magnetar energies $E_p < E_{\text{sn}}$ may play an important role. The resulting peak luminosity is

$$L_{\text{peak}} \sim \frac{E_p t_p}{t_d^2} \sim 5 \times 10^{43} B_{14}^{-2} \kappa_{\text{es}}^{-1} M_5^{-3/2} E_{51}^{1/2} \text{ erg s}^{-1}, \quad (4)$$

which is primarily a function of the magnetic field value, constrained by Equation (3). This shows that $L_{\text{peak}} \sim 10^{43}$ – 10^{45} ergs s^{-1} SNe can be achieved from magnetars with $B_{14} = 1$ – 10 and initial spins in the $P_i = 2$ – 20 ms range. A strict upper limit to the total energy radiated is given by the energy of an NS rotating at a maximal rate of $P_i \sim 1$ ms. The complexity of the energy deposition and subsequent diffusion inhibits using the observed peak luminosities (or radiated energies) to infer anything substantial about the NS equation of state. A more accurate calculation of the peak luminosity will be given in Section 4, but first we describe the dynamical impact of the energy injection.

3. HYDRODYNAMIC IMPACT

Our simple estimate ignores the details of how the deposited energy is distributed throughout the interior of the expanding SNe remnant. Since the dissipation mechanism for the pulsar wind in this medium is poorly understood, we assume the injected magnetar energy is thermalized spherically at the base of the supernova ejecta. In reality, the energy injection may be anisotropic with a jet-like structure (e.g., Bucciantini et al. 2009). The remnant is assumed to be in homologous expansion with a shallow power law density structure in the interior

$$\rho_0(v, t) = \left[\frac{3 - \delta}{4\pi} \right] \frac{M_{\text{ej}}}{v_i^3 t^3} \left(\frac{v}{v_i} \right)^{-\delta}, \quad (5)$$

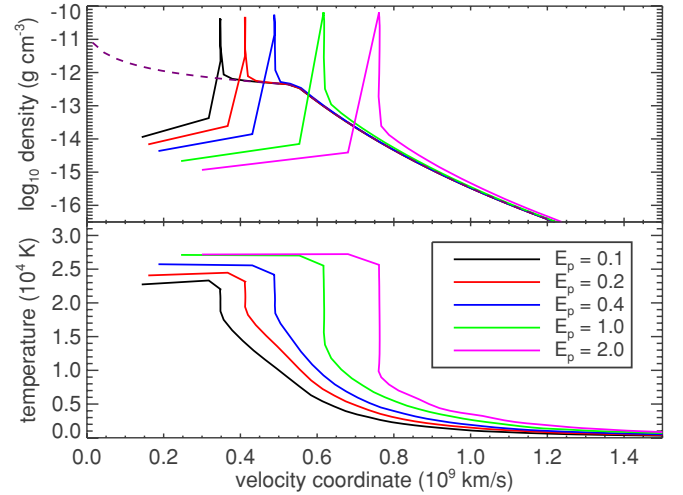


Figure 1. Radiation hydrodynamic calculations of the density (top) and temperature (bottom) of a magnetar-energized supernova, one month after the explosion. The supernova had $M_{\text{ej}} = 5 M_{\odot}$ and $E_{\text{sn}} = 10^{51}$ ergs. The dashed line in the top panel shows the unperturbed density structure, taken from Equation (5). The magnetar had $t_p = 10^5$ s and various values of E_p , labeled in units of 10^{51} ergs.

(A color version of this figure is available in the online journal.)

where $v_t = (2E_{\text{sn}}/M_{\text{ej}})^{1/2}$ is the characteristic ejecta velocity, and the density falls off sharply above v_t .

The central overpressure caused by the energy deposition blows a bubble in the SN remnant, similar to the dynamics studied in the context of pulsar wind nebulae (e.g., Chevalier 1977; Chevalier & Fransson 1992). As this bubble expands, it sweeps up ejecta into a thin shell near the leading shock, leaving the hot, low density interior evident in the one-dimensional radiation hydrodynamic calculations of Figure 1. In multi-dimensional calculations of pulsar wind nebulae, Rayleigh–Taylor instabilities broaden the shell and mix the swept-up material (Jun 1998; Blondin et al. 2001).

The bubble expansion will freeze out in Lagrangian coordinates when the leading shock velocity becomes comparable to the local velocity of the expanding SN ejecta. The postshock pressure is $P = 2\gamma\rho_0 v_s^2/(1+\gamma) = (8/7)\rho_0 v_s^2$ for a strong shock, and the pressure of the energized cavity is $P \approx E_p/3V$, where V is the volume, implying a shock velocity $v_s^2 = 7E_p/32\pi R^3\rho_0$. The shock becomes weak when $v_s \approx R/t$, which determines the final velocity coordinate of the dense shell

$$v_{\text{sh}} \approx v_t \left[\frac{7}{16(3 - \delta)} \frac{E_p}{E_{\text{sn}}} \right]^{1/(5-\delta)}, \quad \text{for } E_p \lesssim E_{\text{sn}}. \quad (6)$$

The weak dependence on E_p , $v_{\text{sh}} \propto E_p^{1/4}$, for $\delta = 1$, places v_{sh} near v_t . The total mass swept up in the shell is $M_{\text{sh}} = M_{\text{ej}}(v_t/v_{\text{sh}})^{3-\delta}$.

The magnetar does not affect the dynamics of the outer layers of the SN ejecta unless $E_p \gtrsim E_{\text{sn}}$, in which case the bubble expands beyond v_t and accelerates more rapidly down the steep outer density gradient. Essentially, all of the ejecta are then swept up into the shell at a final shell velocity

$$v_{\text{sh}} \approx v_t [1 + E_p/E_{\text{sn}}]^{1/2} \quad \text{for } E_p \gtrsim E_{\text{sn}}. \quad (7)$$

Both estimates for v_{sh} assume no radiative losses.

The presence of a dense shell has consequences for the supernova spectra. Initially, the photospheric velocity, v_{ph} , as

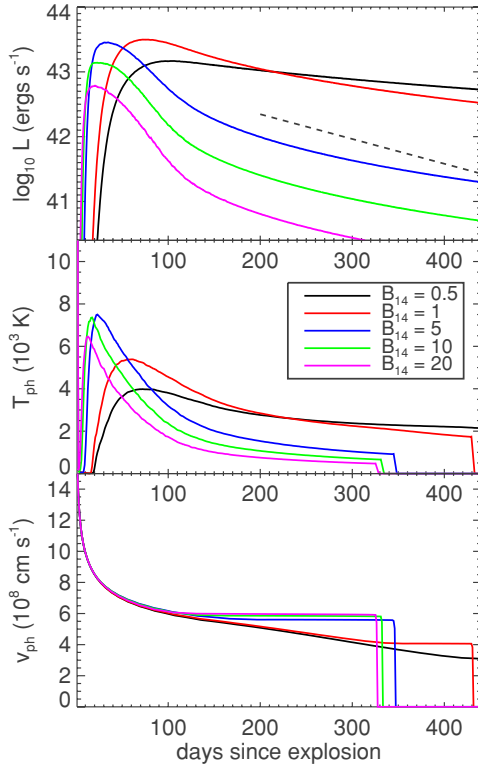


Figure 2. Radiation hydrodynamic calculations of magnetar-energized supernovae with $M_{\text{ej}} = 5 M_{\odot}$, $E_{\text{sn}} = 10^{51}$ ergs, and a density structure given by Equation (5). The magnetar had $P_i = 5$ ms, and various magnetic field strengths. Top panel: bolometric light curves. The dashed line shows, for comparison, the energy deposition from $1 M_{\odot}$ of ^{56}Ni . Middle panel: effective temperature. Bottom panel: velocity of the e^- scattering photosphere at $\tau = 1$.

measured from the Doppler shift of absorption line minima, decreases with time as the outer layers of ejecta become transparent. Once v_{ph} has receded to the shell velocity; however, it will remain constant (Figure 2, bottom panel). The spectra will then be characterized by relatively narrow but blueshifted absorption features, and the spectral evolution will be notably slow. The shell becomes optically thin to electron scattering at a time

$$t_{\tau=1} = 326 M_5 E_{51}^{-1/2} \kappa_{\text{es}}^{1/2} \text{ days.} \quad (8)$$

Recombination may hasten this transition. The electron scattering photosphere drops suddenly to zero after $t_{\tau=1}$, which may cause a sudden change in the spectral appearance at this time. On the other hand, the line opacity in the shell remains optically thick for long after $t_{\tau=1}$, and so the line absorption features will continue to form in the same velocity range. Detailed radiation transfer calculations will be needed to fully describe the spectral evolution.

4. LIGHT CURVES

We now derive analytic expressions for the peak luminosity of a magnetar powered SNe using a one-zone model for the whole remnant. The internal energy, E_{int} , is governed by the first law of thermodynamics

$$\frac{\partial E_{\text{int}}}{\partial t} = -P \frac{\partial V}{\partial t} + L_p(t) - L_e(t), \quad (9)$$

where L_p is the magnetar luminosity and L_e the radiated luminosity. We assume that the magnetar energy is thermalized throughout the remnant, and that radiation pressure dominates,

$P = E_{\text{int}}/3V$. When the volume increases as $V \propto t^3$, Equation (9) becomes

$$\frac{1}{t} \frac{\partial}{\partial t} [E_{\text{int}} t] = L_p(t) - L_e(t). \quad (10)$$

The radiated luminosity, L_e , is approximated from the diffusion equation

$$\frac{L_e}{4\pi R^2} = \frac{c}{3\kappa\rho} \frac{\partial E_{\text{int}}/V}{\partial r} \approx \frac{c}{3\kappa\rho} \frac{E_{\text{int}}/V}{R}, \quad (11)$$

and rewritten using $R = v_f t$, defining the effective diffusion time, t_d

$$L_e = \frac{E_{\text{int}} t}{t_d^2} \quad \text{where} \quad t_d = \left[\frac{3}{4\pi} \frac{M_{\text{ej}} \kappa}{v_f c} \right]^{1/2}, \quad (12)$$

where we take $v_f = [(E_p + E_{\text{sn}})/2M_{\text{ej}}]^{1/2}$ as the final characteristic ejecta velocity. For the simple case where the magnetar injects a constant luminosity $L_p = E_p/t_p$ over a time t_p , and then shuts off, we find

$$L_e(t) = \frac{E_p}{t_p} [1 - e^{-t^2/2t_d^2}], \quad t < t_p;$$

$$L_e(t) = \frac{E_p}{t_p} e^{-t^2/2t_d^2} [e^{t_p^2/2t_d^2} - 1], \quad t > t_p. \quad (13)$$

This light curve peaks at a time t_p , then declines on the characteristic timescale t_d . For $t_p \ll t_d$, $L_{\text{peak}} = E_p t_p / 2t_d^2$, similar to the estimate in Section 2. When $t_p \gg t_d$, we find $L_{\text{peak}} = E_p / t_p$.

More generally, the energy input from the magnetar persists for $t > t_p$, and is given by the spin-down formula

$$L_p(t) = \frac{E_p}{t_p} \frac{l-1}{(1+t/t_p)^l}, \quad (14)$$

where $l = 2$ for magnetic dipole spin-down. The energy input at late times may not be dynamically important, but it enhances the luminosity by continually heating the ejecta similar to radioactive decays. No simple analytic solution for the light curve exists for the general form of $L_p(t)$, but since radiative losses are minimal for times $t < t_d$ we can derive approximate relations by solving Equation (10) for the case $L_e = 0$. The resulting internal energy can be evaluated at time t_d in Equation (12) to estimate the peak luminosity

$$L_{\text{peak}} \approx f \frac{E_p t_p}{t_d^2} \left[\ln \left(1 + \frac{t_d}{t_p} \right) - \frac{t_d}{t_d + t_p} \right], \quad l = 2$$

$$L_{\text{peak}} \approx f \frac{E_p t_p}{t_d^2} \frac{1}{l-2} \left[1 - \frac{t_d/t_p (l-1) + 1}{(1+t_d/t_p)^{l-1}} \right], \quad l > 2, \quad (15)$$

where the correction factor f will be calibrated by comparison to numerical simulation. In general, L_{peak} decreases as l increases, as more of the energy is deposited at earlier times and suffers greater adiabatic losses.

At the peak of the light curve, the radiated luminosity equals the instantaneous magnetar luminosity, $L_{\text{peak}} = L_p(t_{\text{peak}})$, the general expression of ‘‘Arnett’s law’’ (Arnett 1979). This follows from Equation (10), since Equation (12) implies that

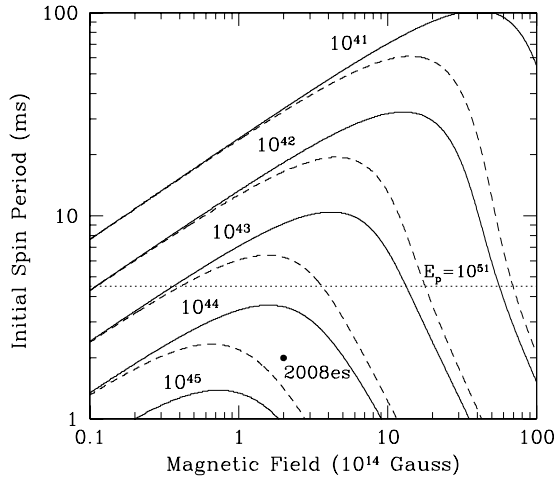


Figure 3. Required B and P_i needed to achieve a given L_{peak} . The lines are contours of constant L_{peak} assuming $E_{\text{sn}} = 10^{51}$ ergs and $M_{\text{ej}} = 5 M_{\odot}$ (solid) or $M_{\text{ej}} = 20 M_{\odot}$ (dashed) from Equation (15). Regions to the right of the knee have $t_p < t_d$, whereas regions to the left of the knee have $t_p > t_d$. The horizontal dotted line shows where $E_p = 10^{51}$ ergs.

the maximum of L_e occurs when $\partial(E_{\text{int}}t)/\partial t = 0$, yielding the time of maximum in the light curve

$$t_{\text{peak}} = t_p \left(\left[\frac{(l-1)E_p}{L_{\text{peak}}t_p} \right]^{1/l} - 1 \right). \quad (16)$$

For $t_p \ll t_d$, the light curve peaks at $t_{\text{peak}} \approx t_d f^{-1/2} [\ln(t_d/t_p) - 1]^{-1/2}$ (assuming $l = 2$), whereas for $t_p \gg t_d$ the peak occurs at $t_{\text{peak}} \approx t_p (\sqrt{2/f} - 1)$.

Figure 2 shows one-dimensional radiation hydrodynamic calculations for $M_{\text{ej}} = 5 M_{\odot}$, $E_{\text{sn}} = 10^{51}$ erg, and central magnetars ($l = 2$) with $P_i = 5$ ms. A gray opacity $\kappa = 0.2 \text{ cm}^2 \text{ g}^{-1}$ was assumed. The simple one-zone model works remarkably well at predicting L_{peak} and t_{peak} , and comparison with the numerical models fixes the value of $f = (l+1)/2$. At late times ($t > t_{\tau=1}$) when the SN becomes optically thin, the light curve tracks the magnetar luminosity, $L \sim t^{-2}$, which is similar to the curve of ^{56}Co decay. Late time measurements of the bolometric light curve could discriminate the two energy sources, though it is not clear that the assumptions of complete thermalization and constant $l = 2$ spin-down will hold at these late times.

In Figure 3, we use Equation (15) to find the locus in the P_i - B space (assuming $l = 2$) needed to reach a certain L_{peak} in a supernova with $E_{\text{sn}} = 10^{51}$ ergs and $M_{\text{ej}} = 5 M_{\odot}$ or $M_{\text{ej}} = 20 M_{\odot}$. A larger M_{ej} increases t_d , which reduces L_{peak} for a given set of magnetar parameters. Magnetars with $P_i \lesssim 5$ ms (below the dotted line) dump enough energy to increase the ejecta velocity, shortening t_d . The lines merge for low B as they asymptote to $L_{\text{peak}} \rightarrow L_p$.

We can also invert the problem and use the measured values of L_{peak} and t_{peak} for an individual supernova to infer B and P_i . Figures 4 and 5 use Equations (15) and (16) to illustrate how L_{peak} and t_{peak} vary with B and P_i . This “mapping” allows for an assessment to be made of the magnetar’s properties and illuminates which numerical calculations should be done. We placed the observed values for 2008es on these plots, motivating the numerical results we show in the following section.

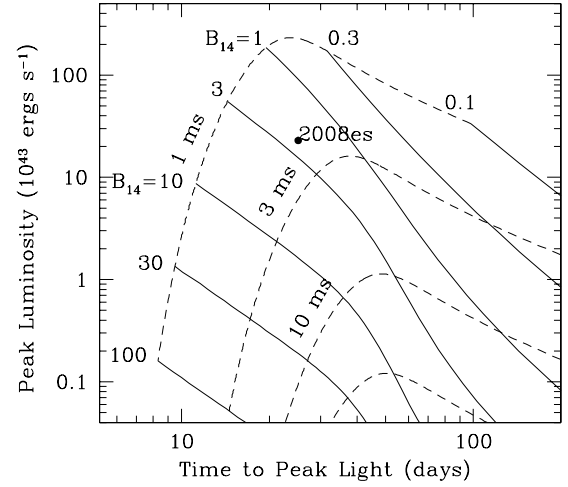


Figure 4. Dependence of L_{peak} and t_{peak} on the initial magnetar spin and B field. The solid lines are for fixed $B_{14} = 100, 30, 10, 3, 1, 0.3,$ and 0.1 and varying spin period, whereas the dashed lines are for a fixed $P_i = 1, 3, 10,$ and 30 ms and varying B . This calculation assumed $E_{\text{sn}} = 10^{51}$ ergs and $M_{\text{ej}} = 5 M_{\odot}$.

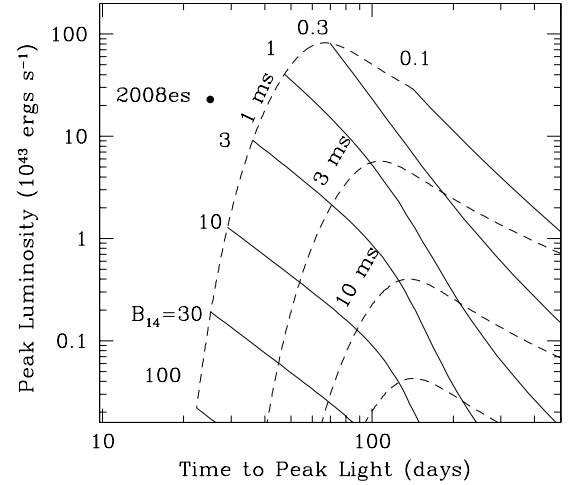


Figure 5. Same as Figure 4, but assuming an ejected mass $M_{\text{ej}} = 20 M_{\odot}$.

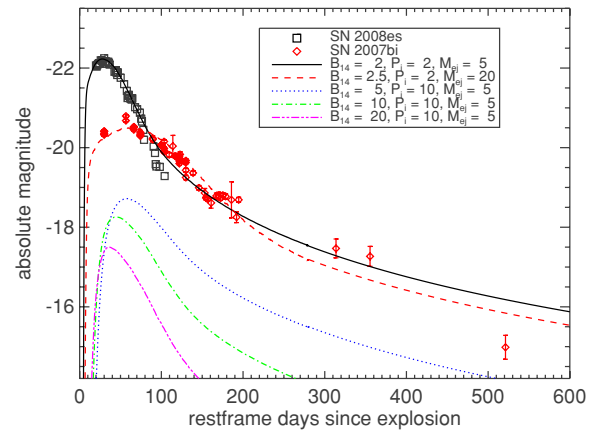


Figure 6. Bolometric light curve calculations of magnetar-energized supernovae compared to observed events. A constant opacity $\kappa = 0.2 \text{ g cm}^{-2}$ is assumed. Black squares show V-band observations of the luminous Type II-L SN2008es (Gezari et al. 2009) with an assumed rise time of 25 days. Red diamonds show R-band observations of the Type Ic SN 2007bi (Gal-Yam et al. 2009) with an assumed rise time of 50 days.

(A color version of this figure is available in the online journal.)

5. DISCUSSION AND CONCLUSION

We have shown that rotational energy deposition from magnetar spin-down with initial spin periods <30 ms can substantially modify the thermal evolution of an expanding SNe remnant. For magnetars in this range, the peak luminosity reaches 10^{42} – 10^{45} erg s $^{-1}$ ($M_{\text{Bol}} = -16.3$ to -23.8), substantially impacting the typical core-collapse SNe light curve, whether it is a Type II or a Ib/c event. The highest luminosities occur when $t_p \sim t_d$, in which case the total energy radiated in the light curve is $E_{\text{rad}} \sim L_{\text{peak}} t_d \sim E_p/3$. The maximal spin of an NS is around 1 ms, so E_{rad} cannot exceed $\sim 10^{52}$ ergs; supernovae radiating larger energies cannot be explained by this mechanism. Though we know that $\sim 10\%$ of core-collapse events make magnetars, we do not know the distribution of initial spin periods, so the prevalence of light curve dominance is difficult to predict. Halpern & Gotthelf (2010) recently reported two additional magnetar candidates in supernova remnants of ages ≈ 1500 and $\approx 27,000$ years, only increasing their prevalence.

For stars with remaining hydrogen, magnetar injection may explain the brighter ($M_B \sim -19$) subclass of Type II-L SNe noted by Richardson et al. (2002), i.e., 1961F, 1979C, 1980K, and 1985L. The light curves of these events are difficult to explain in standard explosion models unless extreme progenitor radii ($R > 2000 R_{\odot}$) are assumed (Blinnikov & Bartunov 1993). Figure 6 shows that a magnetar with relatively modest rotation, $P_i = 10$ ms, in an $M_{\text{ej}} = 5 M_{\odot}$ supernova can reach similar luminosities. Events brighter than $M_{\text{Bol}} = -21$ ($L > 8 \times 10^{43}$ erg s $^{-1}$), such as the ultra-bright Type II-L SN 2005ap (Quimby et al. 2007) and SN 2008es (Gezari et al. 2009; Miller et al. 2009) require an initial magnetar spin of <5 ms. Motivated by Figure 4, we found an excellent fit to the SN 2008es light curve with $B_{14} = 2$, $P_i = 2$ ms, and $M_{\text{ej}} = 5 M_{\odot}$. Such rapidly rotating magnetars must be rare, as Vink & Kuiper (2006) found that the galactic supernova remnants of known magnetars were explained with typical explosion energies of 10^{51} ergs. This rarity is consistent with the specific volume rate of these events; current estimates put them at no more than $\sim 1\%$ (Miller et al. 2009; Quimby et al. 2009) of the local core-collapse rate.

Debate remains (see Klose et al. 2004; Gaensler et al. 2005; Munro et al. 2006; Davies et al. 2009) as to whether magnetars are preferentially formed from the most massive stars that collapse to NSs. If so, then we might see a prevalence of magnetar dominated light curves among the Ib/c SNe, which may partially explain the wide light curve diversity noted in this class. Some extreme SN Ic, such as SN2007bi (Gal-Yam et al. 2009; Young et al. 2010) and SN 1999as (Knop et al. 1999), which remained very bright for a long time, have been claimed to be the pair instability explosion of a $\sim 100 M_{\odot}$ star producing nearly $5 M_{\odot}$ of ^{56}Ni . Figure 6 shows that the early light curve could alternatively be explained for a supernova with $M_{\text{ej}} = 20 M_{\odot}$ forming a magnetar with $B_{14} = 2$, $P_i = 2.5$ ms. At late times (>300 days), our model deviates from the observations, however this could be due to variations in the bolometric correction or thermalization fraction, which are expected to be significant at these epochs. The spectra of SN 1999as revealed a slowly evolving photospheric velocity and narrow, blueshifted absorption features, suggestive of a dense shell like that predicted here (Kasen 2004). On the other hand, the magnetar model may have trouble reproducing the iron emission lines seen in the nebular phase spectrum of SN 2007bi.

Our initial investigations have revealed that if an appreciable fraction of highly magnetic NSs are born rapidly rotating, then we should find evidence for them in the plethora of supernova surveys, such as the Palomar Transient Factory (Law et al. 2009). Many open questions remain on the theoretical side, especially how the outgoing pulsar wind thermalizes in the remnant, whether there are substantial jet-like asymmetries or Rayleigh–Taylor instabilities, and how these could manifest themselves in the observed spectra and polarization both at late times and during the photospheric phase. Our work has outlined the regimes of relevance, and will guide future large-scale computations through parameter space in an informed manner.

We thank David Kaplan, Eliot Quataert, and Stan Woosley for helpful discussions. Support for D.K. was provided by NASA through Hubble fellowship grant No. HST-HF-01208.01-A awarded by the Space Telescope Science Institute, which is operated by the Association of Universities for Research in Astronomy, Inc., for NASA, under contract NAS 5-26555. This research has been supported by the DOE SciDAC Program (DE-FC02-06ER41438) and by the National Science Foundation under grants PHY 05-51164 and AST 07-07633.

REFERENCES

- Arnett, W. D. 1979, *ApJ*, 230, L37
Arons, J. 2003, *ApJ*, 589, 871
Blinnikov, S. I., & Bartunov, O. S. 1993, *A&A*, 273, 106
Blondin, J. M., Chevalier, R. A., & Frierson, D. M. 2001, *ApJ*, 563, 806
Bodenheimer, P., & Ostriker, J. P. 1974, *ApJ*, 191, 465
Bucciantini, N., Quataert, E., Metzger, B. D., Thompson, T. A., Arons, J., & Del Zanna, L. 2009, *MNRAS*, 396, 2038
Chevalier, R. A. 1977, in *Astrophys. Space Sci. Libr.* 66, *Supernovae*, ed. D. N. Schramm (Berlin: Springer), 53
Chevalier, R. A., & Fransson, C. 1992, *ApJ*, 395, 540
Davies, B., Figer, D. F., Kudritzki, R., Trombly, C., Kouveliotou, C., & Wachter, S. 2009, *ApJ*, 707, 844
Duncan, R. C., & Thompson, C. 1992, *ApJ*, 392, L9
Gaensler, B. M., McClure-Griffiths, N. M., Oey, M. S., Haverkorn, M., Dickey, J. M., & Green, A. J. 2005, *ApJ*, 620, L95
Gaffet, B. 1977a, *ApJ*, 216, 565
Gaffet, B. 1977b, *ApJ*, 216, 852
Gal-Yam, A., et al. 2009, *Nature*, 462, 624
Gezari, S., et al. 2009, *ApJ*, 690, 1313
Halpern, J. P., & Gotthelf, E. V. 2010, *ApJ*, 710, 941
Jun, B. 1998, *ApJ*, 499, 282
Kasen, D. N. 2004, PhD thesis, Univ. of California, Berkeley
Klose, S., et al. 2004, *ApJ*, 609, L13
Knop, R., et al. 1999, *IAU Circ.*, 7128, 1
Kouveliotou, C., et al. 1998, *Nature*, 393, 235
Law, N. M., et al. 2009, *PASP*, 121, 1395
Maeda, K., et al. 2007, *ApJ*, 666, 1069
Miller, A. A., et al. 2009, *ApJ*, 690, 1303
Munro, M. P., et al. 2006, *ApJ*, 636, L41
Quimby, R. M., Aldering, G., Wheeler, J. C., Höflich, P., Akerlof, C. W., & Rykoff, E. S. 2007, *ApJ*, 668, L99
Quimby, R. M., et al. 2009, arXiv:0910.0059
Richardson, D., Branch, D., Casebeer, D., Millard, J., Thomas, R. C., & Baron, E. 2002, *AJ*, 123, 745
Thompson, C., & Duncan, R. C. 1993, *ApJ*, 408, 194
Thompson, T. A., Chang, P., & Quataert, E. 2004, *ApJ*, 611, 380
Uzdensky, D. A., & MacFadyen, A. I. 2007, *ApJ*, 669, 546
Vink, J., & Kuiper, L. 2006, *MNRAS*, 370, L14
Wheeler, J. C., Yi, I., Höflich, P., & Wang, L. 2000, *ApJ*, 537, 810
Woods, P. M., & Thompson, C. 2006, in *Cambridge Astrophys. Ser.* 39, *Compact Stellar X-ray Sources*, ed. W. Lewin & M. van der Klis (Cambridge: Cambridge Univ. Press), 547
Woosley, S. 2009, arXiv:0911.0698
Young, D. R., et al. 2010, *A&A*, 512, A70